Study of the Mutual Influence of the El Niño–Southern Oscillation Processes and the North Atlantic and Arctic Oscillations

I. I. Mokhov[a] and D. A. Smirnov[b]

[a] *Oboukhov Institute of Atmospheric Physics, Russian Academy of Sciences, Pyzhevskii per. 3, Moscow, 119017 Russia*
e-mail: mokhov@ifaran.ru
[b] *Institute of Radio Engineering and Electronics (Saratov Branch), Russian Academy of Sciences,*
Zelenaya ul. 38, Saratov, 410019 Russia
e-mail: smirnovda@info.sgu.ru

Received November 9, 2005

Abstract—On the basis of the nonlinear techniques for the estimation of coupling between oscillatory systems from time series, we investigate the dynamics of climatic modes characterizing global and Northern Hemisphere (NH) processes. The North Atlantic Oscillation (NAO) and Arctic Oscillation indices and the El Niño–Southern Oscillation (ENSO) indices are analyzed in terms of the most reliable data from 1950 through 2004 and earlier data since the 19th century. These indices characterize changes in NH atmospheric pressure (specifically, sea-level pressure in the North Atlantic and NH extratropical latitudes as a whole) and in equatorial Pacific sea-surface temperature and sea-level pressure to which the strongest variations of global surface temperature and global climate on interannual time scales and of regional climatic anomalies in the NH are linked. The methods used are based on phase-dynamics modeling and nonlinear prediction models (a nonlinear version of *Granger causality*). From both methods and various ENSO indices, the inference about the ENSO effect on the NAO during the latter half of the 20th century and in the early 21st century is made with confidence probability of at least 0.95. The influence is characterized by a time delay of about two years. No inverse influence is found with a similar degree of reliability. Results of estimating the coupling between the ENSO and the NAO depend on the type of index that is used to describe the NAO. The ENSO effect on the NAO is detected with sufficient confidence when the NAO index is chosen to be a larger scale characteristic. However, when a more local index of the NAO is used, no statistically significant coupling to the ENSO is found. Increasing the length of the analyzed ENSO and NAO series (over more than 100 yr) does not lead to any more reliable detection of coupling. Analysis of the data for different time intervals during 1950–2004 has revealed a strengthening of the ENSO effect on the NAO, although this inference is not reliable.

DOI: 10.1134/S0001433806050069

1. INTRODUCTION

The El Niño–Southern Oscillation (ENSO), North Atlantic Oscillation (NAO), and Arctic Oscillation (AO) processes represent the leading modes of interannual climate variability for the Earth as a whole and for the Northern Hemisphere (NH) [1, 2]. The detection of mechanisms that form these processes is a problem of great fundamental and practical importance. The issue of the existence and character of the mutual influence of the ENSO, NAO, and AO is of special interest. For its investigation, different analysis methods have been applied, such as the calculation of cross-correlation functions, Fourier coherence, and wavelet coherence, with the use of time series of various ENSO, NAO, and AO indices from sea-surface temperature (SST) and sea-level pressure data [1–30]. An important indicator of the global processes, including the influence of the ENSO, NAO, and AO, may be hydrologic-cycle variations in the Caspian Sea basin with corresponding changes in its level [16, 17].

The NAO index defined as the normalized sea-level pressure difference between the Azores (the Azores High) and Iceland (the Icelandic Low) is widely used [5, 31]. The NAO can also be characterized by different expansion modes of the NH atmospheric fields of pressure, geopotential, and SST, in particular, throught the use of the empirical orthogonal function (EOF) expansion. In [32], for example, the NAO is characterized by the first mode of expansion of the NH middle-troposphere 500-hPa geopotential height field on the basis of rotated principal component analysis (RPCA), described, for example, in [9]. The NAO index from [32] is thus a hemispheric-scale characteristic (mode), i.e., a larger scale characteristic than that presented in [5, 31]. The NAO is closely linked to the Arctic Oscillation, which characterizes a circulation regime of the atmosphere not only of the high latitudes but also in much of the NH, except the tropical latitudes (north of 20° N) [9]. In [32], the NAO index is defined as the first mode in the

EOF expansion of the 1000-hPa geopotential height field in the NH.

The El Niño indices T(Niño3), T(Niño3.4), T(Niño4), and T(Niño1+2) characterize SST in the corresponding equatorial regions of the Pacific Ocean (Niño3, 5° N–5° S, 150° W–90° W; Niño3.4, 5° N–5° S, 170° W–120° W; Niño4, 5° N–5° S, 160° E–150° W; and Niño1+2, 0°–10° S, 90° W–80° W [32]). The index of the Southern Oscillation (SO) is calculated as the normalized sea-level pressure difference in the Pacific basin, between the island of Tahiti and Darwin (Australia) [31, 32].

It should be noted that the time series with the most reliable data for characteristics of these processes, in particular, for the ENSO temperature indices, are comparatively short, from the second half of the 20th century and onward (from 1950 through 2004, with a total of 660 monthly means). The processes are very complicated, so that it is not easy to draw reliable inferences about their coupling.

In recent years, new methods for diagnosis of the coupling between oscillatory systems from time series have been developed within the framework of nonlinear dynamics. These can be divided into two large groups [33, 34]: some are based on the estimation of the interdependence in the reconstructed spaces of states [35–44], and others are based on analysis of the phase dynamics of oscillations [45–53]. These methods are able to identify complicated and rather weak nonlinear interactions and their "direction." It is shown in [34] that nonlinear methods of each group have their own efficiency conditions, and it is reasonable to use different methods simultaneously to more completely extract the information about interactions that is contained in the observed signals.

The goal of the study is a systematic investigation of the mutual influence of the ENSO, NAO, and AO from the time series of their various indices on the basis of nonlinear methods of coupling diagnosis (early results of such an investigation were reported briefly in [54]). Section 2 describes the experimental data and methods to be used. Section 3 presents the main results. These are summarized and discussed in Section 4.

2. EXPERIMENTAL DATA AND METHODS OF ANALYSIS

2.1. Experimental Data

For analysis of the ENSO, NOA, and AO processes in 1950–2004, the following indices were used:

(i) for the NAO process, the NAO indices from [32] and [31];

(ii) for the AO, the AO index from [32];

(iii) for the ENSO, the temperature indices T(Niño3), T(Niño3.4), T(Niño4), and T(Niño1+2) from [32] and the SO index from [32] and [31]. We

considered the indices themselves T(Niño3), T(Niño3.4), T(Niño4), and T(Niño1+2) as well as their anomalies, i.e., the signals with the eliminated annual cycle.

Longer series were analyzed for the NAO index (1821–2004), T(Niño3) (1871–1997), and SO index (1866–2004) [31, 32, 18, 19]. Thus, results have been obtained for short series (since 1950) as well as for longer series (since 1871 or 1866).

The distinctive feature of the problem is a relatively short duration of analyzed series. For typical time scales (2 years or more), the maximum number of characteristic periods in the time series is 24 for shorter periods and 65 for the longer ones. This makes it difficult to draw inferences with a high confidence probability. In estimating the coupling between the processes, only results with a confidence probability of at least 0.95, i.e., at the significance level $p < 0.05$, were considered to be statistically significant.

2.2. Phase-Dynamics Approach

The main idea of the method is to estimate how strongly the future evolution of the phase of one system depends on the current value of the phase of the other system. For this purpose, from the original time series of two systems $\{x_1(t_1), …, x_1(t_N)\}$ and $\{x_2(t_1), …, x_2(t_N)\}$ ($t_i = i\Delta t$, with Δt being a sampling interval, for which $\Delta t = 1$ is set for simplicity), one can construct time series of phases of their oscillations $\{\phi_1(t_1), …, \phi_1(t_N)\}$ and $\phi_2(t_1), …, \phi_2(t_N)\}$, whereby a mathematical model can be developed [49, 53].

There are different methods for calculation of oscillation phases [55–58]. A classical method [55] of calculating a phase of the signal $X(t)$ is to find a complex analytic signal $Z(t) = X(t) + jY(t)$, where Y is the Hilbert conjugate signal: $Y(t) = P.V. \int_{-\infty}^{\infty} \frac{X(t')dt'}{\pi(t - t')}$, where $P.V$ is the principal value of the improper integral. The phase $\phi(t)$ of the signal $X(t)$ is determined as an argument of $Z(t)$, i.e., the angle of rotation of a radius vector on the complex (Re Z, Im Z) plane. If the phase is determined in the interval $[0, 2\pi)$, it is referred to as wrapped. In what follows, we are dealing only with an unwrapped phase $\phi(t)$, which increases by 2π per each full rotation of the radius vector. For $X(t) = \cos(\omega t + \varphi)$, for example, the Hilbert conjugate signal is $Y(t) = \sin(\omega t + \varphi)$ and the phase is $\phi(t) = \omega t + \varphi$.

This approach, however, has a clear physical meaning only for the signals with a pronounced main rhythm (narrowband signals). In this case, the phase characterizes the repetition in the signal. Roughly speaking, it varies by 2π in the interval between two consecutive minima. If the spectrum of a signal contains many peaks at different frequencies, band-pass filtering is usually used to isolate a certain rhythm and

the approach described is applied to a filtered signal. It is desirable to justify the choice of a filter band from a physical point of view. In practice, the Hilbert transform is often performed in a frequency domain, for which all phases in the Fourier transform of the signal X are shifted by $-\pi/2$ and an inverse Fourier transform is performed. In any case, the calculated phase values near the beginning and end of the time series are distorted (edge effect) and phase values should be rejected for ten characteristic periods from each "end" of the time series [48].

Since in this study we analyze relatively short time series of climatic indices, the removal of such a large amount of data is quite undesirable. For this reason, another technique was used to construct an analytic signal [57], which is identical to band-pass filtering and the subsequent Hilbert transform but suffers less from edge effects. This is a complex wavelet transform

$$Z(t) = \frac{1}{\sqrt{s}} \int_{-\infty}^{\infty} X(t')\psi^*((t-t')/s)dt', \quad (1)$$

where the complex wavelet function is a Morlet transform $\psi(\eta) = \pi^{-1/4}\exp(-j\omega_0\eta) \times \exp(-\eta^2/2)$, the asterisk means the complex conjugate, and s is a fixed time scale. The phase is the argument Z. This approach is equivalent to band-pass filtering of the original signal around the frequency $f \approx \dfrac{\omega_0}{2\pi s}$, with a bandwidth determined by the parameter ω_0. When $\omega_0 = 6$ [59, 60], which is also used here, a bandwidth corresponds roughly to 1/4 of the central frequency $f \approx 1/s$. Edge effects occur in intervals of length $\sqrt{2}s$ [59], i.e., about 1.4 characteristic periods.

The form of a mathematical model is chosen from the following considerations. For a wide range of situations, the phase dynamics of oscillators that exhibit a pronounced main rhythm is adequately described by stochastic differential equations, as in [47],

$$d\phi_k/dt = \omega_k + G_k(\phi_1, \phi_2) + \xi_k(t), \quad k = 1, 2, \quad (2)$$

where ω_k represents parameters that determine angular frequencies of oscillations and $\xi_k(t)$ are independent Gaussian white noises with zero mean and autocorrelation functions $\langle\xi_k(t)\xi_k(t')\rangle = 2D_k\delta(t-t')$. In the treatment of discrete time series, it is convenient to use a difference form of equations

$$\Delta\phi_k(t) = F_k(\phi_1(t), \phi_2(t), \mathbf{a}_k) + \varepsilon_k(t), k = 1, 2, \quad (3)$$

where $\Delta\phi_k(t) \equiv \phi_k(t+\tau) - \phi_k(t)$ is a phase increment per finite time τ, $\varepsilon_k(t)$ are zero-mean noises, F_k are trigonometric polynomials, and $\mathbf{a}_k$ are vectors of their coefficients.

To construct model (3), it is necessary to specify the interval τ (usually taken equal to the characteristic period of oscillations [49]) and orders of the polynomials F_k (third-order polynomials are further used, following [49, 50, 53]). The estimates of coefficients $\hat{\mathbf{a}}_k$ are determined with a least-squares method (LSM), i.e., through minimization:

$$\sigma^2_{\phi, k} = \frac{1}{N-\tau}\sum_{i=1}^{N-\tau}(\Delta\phi_k(t_i)$$
$$- F_k(\phi_1(t_i), \phi_2(t_i), \mathbf{a}_k)^2 \longrightarrow \min, \quad k = 1, 2. \quad (4)$$

Next, intensities of influence of the oscillators on each other are calculated from the coefficient estimates $\hat{\mathbf{a}}_k$.

If the "true" equations of phase dynamics were known a priori, the strength of influence of the second system on the first one, c_1, could be determined by the steepness of the dependence of F_1 on ϕ_2, while that of the first system on the second one, c_2, could be determined in a similar way:

$$c^2_{1, 2} = \frac{1}{2\pi^2}\int_0^{2\pi}\int_0^{2\pi}(\partial F_{1, 2}(\phi_1, \phi_2, \mathbf{a}_{1, 2})/\partial\phi_{2, 1})^2 d\phi_1 d\phi_2. \quad (5)$$

The directionality index is determined by the difference of c_1 and c_2. These would have been the "true" coupling characteristics. From the time series, however, one can obtain only the estimates of coefficients $\hat{\mathbf{a}}_k$, from which the estimates of c_1 and c_2 are to be calculated. The most straightforward way is to use formula (5) and substitute $\hat{\mathbf{a}}_k$ instead of the true values $\mathbf{a}_k$. However, such estimates of $\hat{c}_{1, 2}$ appear to be accurate only for very long stationary signals (about 5000 characteristic periods in length for a sampling frequency of 10–20 points per period and a moderate noise level [49, 53]). For shorter time series with limited reliable data, these estimates are biased. In [53], new estimators $\hat{\gamma}_{1, 2}$ for $c^2_{1, 2}$ were presented (see Appendix A). Formulas for their 95% confidence intervals were also obtained in the form [$\hat{\gamma}_k - 1.6\hat{\sigma}_{\hat{\gamma}_k}$, $\hat{\gamma}_k + 1.8\hat{\sigma}_{\hat{\gamma}_k}$], where $\hat{\sigma}_{\hat{\gamma}_k}$ are calculated from the same short series. The estimators $\hat{\gamma}_{1, 2}$ are unbiased and provide the frequency of erroneous inferences about the presence of mutual influence of the systems at a level no higher than 0.025 (see Appendix A) even for relatively short time series but desirably with a length of at least 50 characteristic periods [53]. According to additional studies with reference oscillators, the estimators (controlled probability of erroneous conclusions) also remain applicable for shorter series of a length up to 20 characteristic periods if the phase coherence coefficient [46] $\rho \equiv |\langle\exp(j(\varphi_1(t) - \varphi_2(t)))\rangle_t|$, where the angle brackets denote time averaging, calculated from such a short series does not exceed 0.4. In this case, a near-uniform distribution of the experi-

mental points in the square $[0, 2\pi] \times [0, 2\pi]$ on the plane of wrapped phases ($\phi_1 \bmod 2\pi$, $\phi_2 \bmod 2\pi$) takes place.

In analysis of the climatic indices, we used the method described above, the models being constructed with the possible delay in coupling [6] of the form

$$\Delta\phi_{1,2}(t) = F_{1,2}(\phi_{1,2}(t), \phi_{2,1}(t+\Delta), \mathbf{a}_{1,2}) + \varepsilon_{1,2}(t), \quad (6)$$

where Δ is the time shift between series. The negative value of Δ means a delayed coupling. The coupling characteristics $\hat{\gamma}_{1,2}(\Delta)$ were calculated for Δ varying from some negative number large in absolute value to $\Delta = \tau$. The values $\Delta > \tau$ have no physical meaning because they denote the influence of future values on the current ones. Accordingly, the coefficient ρ was also calculated depending on Δ: $\rho(\Delta) = |\langle\exp(j\phi_1(t) - \phi_2(t+\Delta))\rangle_t|$. Only the values of $\hat{\gamma}_{1,2}(\Delta)$ corresponding to $\rho(\Delta) < 0.4$ were taken into account.

2.3. Method Based on Nonlinear Prediction Models

It is often reasonable to analyze not only phases but also amplitudes. The traditional and simplest version is the estimation of cross-correlation functions. To obtain more complete information, it is possible to use nonlinear methods based on the analysis of interdependences in the spaces of states. Out of the latter, we have chosen a method of nonlinear prediction models [42, 44], which is an extension of the linear approach to identification of causality proposed by Granger [62] (see also [63–65]) and lies in the following. From the available time series $\{x_1(t_1), ..., x_1(t_N)\}$ and $\{x_2(t_1), ..., x_2(t_N)\}$, we construct prediction models, individual and coupled. If the prediction of the dynamics of the first system can be substantially improved via incorporation of values of the variable of the second system and such an improvement cannot be achieved via complication of an individual system, the second system has an influence on the first system. We used the following specific realization.

To estimate the influence of the second system on the first one, an individual model is constructed

$$x_1(t_n) = f_1(x_1(t_{n-1}), x_1(t_{n-2}), ..., x_1(t_{n-d_1}), \mathbf{a}_0), \quad (7)$$

where f_1 is a polynomial of order K and d_1 is the dimension of the model. The coefficient estimates $\hat{\mathbf{a}}_0$ are found through the LSM. The unbiased estimate of the mean square of the prediction error is

$$\sigma_1^2 = \frac{1}{N' - P_1} \times \sum_{i=i_0+1}^{N}(x_1(t_i) - f_1(x_1(t_{i-1}), x_1(t_{i-2}), ..., x_1(t_{i-d_1}), \hat{\mathbf{a}}_0))^2, \quad (8)$$

where $i_0 = \max(d_1, d_2)$, $N' = N - i_0$, and $P_1 = (d_1 + K)!/d_1!K!$ is the number of coefficients of the model. Then, using the two time series, we construct a model of the form

$$x_1(t_n) = g_1(x_1(t_{n-1}), ..., x_1(t_{n-d_1}), x_2(t_{n-1}), ..., x_2(t_{n-d_2}), \mathbf{a}), \quad (9)$$

where d_2 is the number of x_2 values taken into account, g_1 is a polynomial of order K, and the coefficient estimates $\hat{\mathbf{a}}$ are calculated through the LSM. The prediction error of the coupled model is given by

$$\sigma_{2\to1}^2 = \frac{1}{N' - P_2}\sum_{i=i_0+1}^{N}(x_1(t_i) - g_1(x_1(t_{i-1}), ..., x_1(t_{1-d_1}), x_2(t_{i-1}), ..., x_2(t_{i-d_2}), \hat{\mathbf{a}}))^2, \quad (10)$$

where $P_2 = (d_1 + d_2 + K)!/(d_1 + d_2)!K!$ is the number of coefficients of the coupled model.

The improvement of the prediction of the series x_1 with consideration for the series x_2 is characterized by the difference of the errors squared $PI_{2\to1} = \sigma_1^2 - \sigma_{2\to1}^2$. To estimate the significance of the error improvement obtained from the time series, one should keep in mind that, for uncoupled processes $x_1(t)$ and $x_2(t)$ with Gaussian white noise responsible for the prediction errors, the normalized quantity

$$F_{2\to1} \equiv \frac{\dfrac{1}{P_2 - P_1}(\sigma_1^2(N' - P_1) - \sigma_{2\to1}^2(N' - P_2))}{\sigma_{2\to1}^2} \quad \text{has}$$

an F-distribution with $(P_2 - P_1, N' - P_2)$ degrees of freedom. The significance of positive $PI_{2\to1}$ can then be tested from $F_{2\to1}$ via an F-test [66, 67]. If $PI_{2\to1}$ is significant at the level p, we must allow the presence of the influence of x_2 on x_1 with the confidence probability $(1 - p)$. Everything is analogous for the influence $1 \longrightarrow 2$.

The improvement of the prediction and the model coefficients were calculated for different time shifts Δ between the series, i.e., for models of the form

$$x_1(t_n) = g_1(x_1(t_{n-1}), ..., x_1(t_{n-d_1}), x_2(t_{n-1+\Delta}), ..., x_2(t_{n-d_2+\Delta}), \mathbf{a}), \quad (11)$$

with allowance for the possible delay Δ in coupling. The delay Δ was changed from a negative integer large in absolute value to 0. The dimensions of the models and the order K were allowed to vary.

It is desirable to use multivariate models with high-order polynomials in order to describe the observed complicated dynamics more adequately. However, this method requires enormous volumes of data. In our
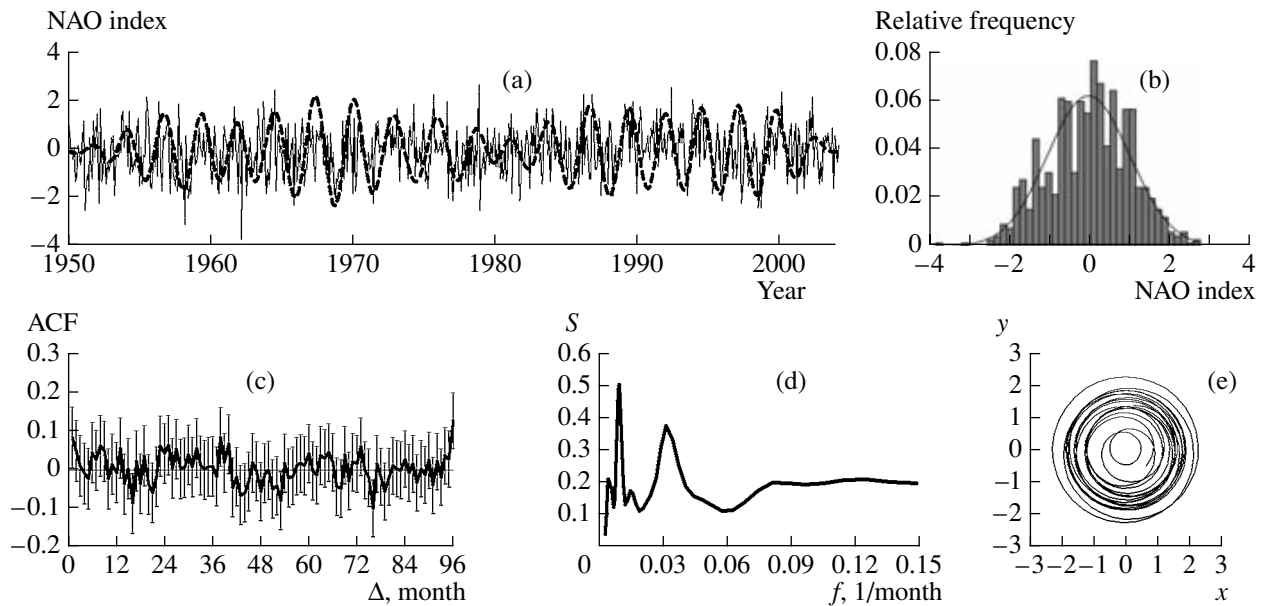
Fig. 1. Individual characteristics of the NAO index from [32] (short series, 1950–2004): (a) gray color denotes the original time series and the dashed line represents the real part of the wavelet transform with a time scale $s = 32$ months or a band-pass filtered signal; (b) histogram, where the solid line is the approximation by a Gaussian; (c) ACF and its 95% pointwise confidence intervals, with a halfwidth being a double error estimate according to Moran [67]; (d) global wavelet spectrum; and (e) trajectory on a complex plane for a scale $s = 32$ months.

case of relatively short series, we have to restrict ourselves to low-dimensional models with low-order polynomials, i.e., to a small number of free parameters, so that the estimates of the latter will be more stable. We used d_1, d_2, and K in the range from 0 to 3.

Finally, we have analyzed cross-correlation functions and prediction models for time series containing only average winter values of each index. These time series are even shorter than those based on the monthly means and contain only one value per year, so that the reliability of results can be strongly reduced because of poor statistics. On the other hand, since the ENSO, NAO, and AO indices characterize processes that are most clearly defined during the Northern Hemisphere winter, there is reason to assume that the identification of only winter values may produce an effect analogous to a decrease in the noise level. This is desirable for a more confident estimation of the mutual influence.

3. RESULTS

3.1. Analysis of Phase Dynamics of ENSO and NAO Processes

Among the most adequate and often-used indicators of El Niño events are the indices T(Niño3) and T(Niño3.4). The calculated individual characteristics of the NAO index [32] and T(Niño3.4) for the 1950–2004 period are shown in Figs. 1 and 2 (in Figs. 2a and 2b, the results are given after the reduction to zero mean).

In the estimation of the autocorrelation function (ACF) of the NAO index, there are almost no significant correlations (Fig. 1c), but a periodic component with a period of about 30 months can be visually detected (not confidently). The global wavelet spectrum of the NAO index obtained with a Morlet wavelet is shown in Fig. 1d. The smoothed estimate of the power spectrum [59] reveals peaks corresponding to cyclicity with a period of 32 months, 108 months, and other values. One might assume that oscillatory processes for which the phase can be adequately determined are associated precisely with these peaks.

For the T(Niño3.4) index from [32] for the same 1950–2004 period, the ACF drops more slowly and correlations for delays from 1 to 6 months are significant (Fig. 2c). A component with a period of about 60 months is detected visually (with no confidence either). The wavelet spectrum reveals peaks corresponding to scales of 12 months, 69 months, etc.

In analysis, the values s in (1) corresponding to different peaks in both spectra were used to obtain the NAO and ENSO phases of "different rhythms." The interaction among all these rhythms was estimated pairwise via the phase-dynamics approach. The only version in which informative inferences about the presence of coupling were obtained is a "rhythm" with $s = 32$ months for both signals. In Figs. 1a and 2a, the dashed line shows time realizations of the real part of the wavelet coefficient corresponding to $s = 32$. Trajectories of both processes on a complex plane are shown in Figs. 1 and 2: the rotation of the radius vec-
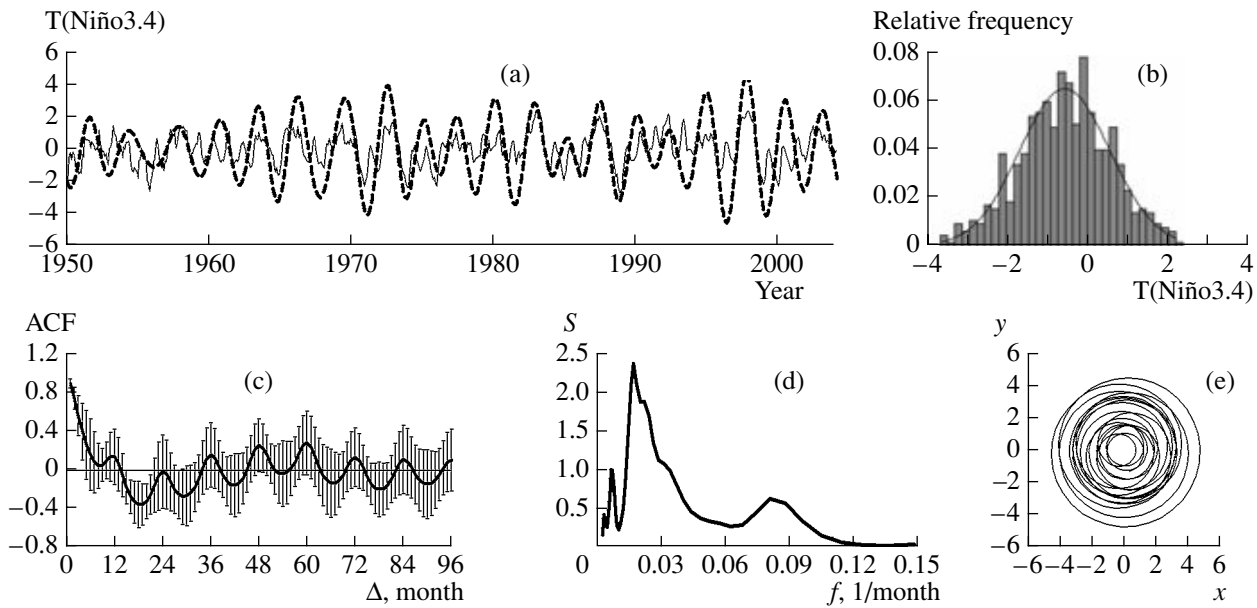
Fig. 2. Individual characteristics of T(Niño3.4) (from [32] for 1950–2004). Notations are the same as in Fig. 1.

tor around the origin of coordinates takes place, so that the phases of both signals for a given rhythm are well defined.

Results of constructing models (6) are displayed in Fig. 3. The dependence of the mean-square errors $\sigma_{\phi,1}^2$ and $\sigma_{\phi,2}^2$ of phase-dynamics model (6) on the method's parameter τ for a fixed $\Delta = 0$ is shown in Figs. 3a and 3b. This dependence for moderate τ values is approximately linear, a result that confirms the adequacy of the model of type (6) [53]. The value of $\sigma_{\phi,k}^2$ for $\tau = s = 32$ is the effective phase diffusion coefficient multiplied by 2τ [69]. For the selected rhythm, it is an order of magnitude greater for T(Niño3.4); i.e., phase diffusion for T(Niño3.4) is substantially stronger than that for the NAO from [32]. This means that the probability of detecting the influence of the NAO on T(Niño3.4), if any, is less because of a stronger effective noise in the phase dynamics of T(Niño3.4).

Figure 3 shows experimental points on the plane of wrapped phases for $\Delta = 0$. The distribution is approximately uniform, and the phase coherence coefficient is not large, $\rho \approx 0.25$, thus indicating that the phase-dynamics approach is applicable for $\Delta = 0$. However, ρ becomes greater than 0.4 when $\Delta < -30$, and the values of coupling estimates cannot be taken into account (Fig. 3f). The estimate of the strength of the influence of the El Niño on the NAO is pointwise significant for the interval $-30 < \Delta < 0$ and takes a maximum value when $\Delta = -24$ months (Fig. 3d). How reliably can one draw a conclusion about the influence of El Niño on the NAO? Its confidence probability can be estimated from the following considerations. The values of

$\hat{\gamma}_1(\Delta)$ for close Δ values are strongly correlated. This is evident in the smoothness of the dependence $\hat{\gamma}_1(\Delta)$ (Fig. 3d). The values of the estimate of $\hat{\gamma}_1(\Delta)$ separated in Δ by an interval larger than τ can be considered statistically independent. In the given case, $\tau = 32$ and the interval of Δ taken into account includes values from -30 to 32. Therefore, two groups of estimate values are independent of each other (with a strong cross-correlation within each group): for Δ from the intervals $[-30, 0]$ and $[0, 32]$. The probability of a random false inference about coupling, based on an individually significant $\hat{\gamma}_1$ only in one of these groups, is equal to a pointwise probability of error of 0.025. The probability of a false inference based on an individually significant $\hat{\gamma}_1$ at least in one of these two groups (the required total error probability) is approximately equal to the sum of the probabilities of individual errors due to the smallness of the latter and amounts to 0.05. Consequently, the inference about the influence of El Niño on the NAO can be drawn with a 0.95 confidence probability. The most probable delay is about 24 months, but this conclusion is not sufficiently reliable. No indications of the inverse influence of the NAO on ENSO were found from phase-dynamics modeling results from [32] (Fig. 3e).

It should be noted that large values of the phase coherence index for $\Delta < -30$ are not indicative of a strong coupling with the corresponding delay. For such short series and close fundamental oscillation frequencies, the probability that a large value of ρ can be obtained for uncoupled processes is very high
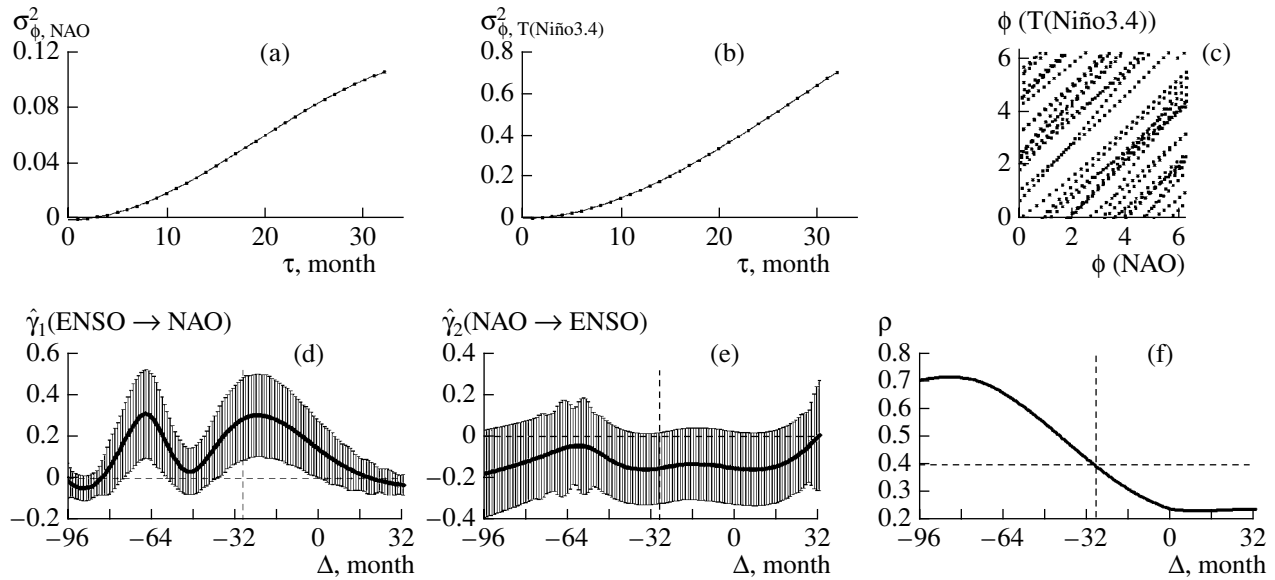
Fig. 3. Analysis of coupling between the NAO index and T(Niño3.4) from [32] by the method of phase-dynamics modeling for rhythms with $s = 32$ months: (a, b) dependence of the residual error of phase-dynamics model (6) on τ, usually taken equal to the characteristic period, for each of the processes; (c) experimental points on the plane of wrapped phases; (d, e) estimate of the strength of the influence of the processes on each other, where $\tau = 32$ (gray color shows pointwise confidence intervals, and only values on the left of the vertical dashed line correspond to the area of applicability of the method); (f) phase coherence index (the dashed line is a threshold value 0.4).
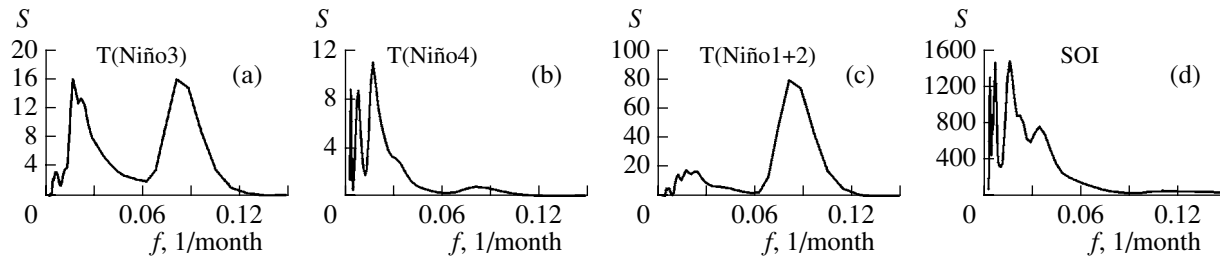

Fig. 4. Global wavelet spectra for ENSO indices T(Niño3), T(Niño4), and T(Niño1+2) and the SO index from [32] for 1950–2004.

(above 0.5, as shown by the results of numerical experiments with reference oscillators).

During analysis of other rhythms of the NAO and T(Niño3.4) indices from [32], conclusive inferences about coupling failed to be made. For example, for 12- and 32-month rhythms in different combinations, the values of $\hat{\gamma}_{1,2}(\Delta)$ were found to be insignificant. For 69- and 108-month rhythms, the time series are too short for the method to be applied, shorter than 20 characteristic periods.

Using other ENSO indices instead of T(Niño3.4) leads to roughly the same conclusions as those above. Global wavelet spectra of the signals are shown in Fig. 4. They are slightly different from one another, so that one can expect somewhat "independent" information of the analysis of these indices. Nevertheless, in the frequency band corresponding to 28- to 36-month

scales, which gives the most interesting results, the values of the Fourier coherence among all the ENSO indices are large, about 0.9–0.95 for all pairs of the indices except for the pairs with T(Niño1+2), where the coherence is about 0.85. There are in-phase oscillations of the temperature indices in the indicated frequency band, and the AO index oscillates in antiphase with them. The plots for the estimates of coupling with the NAO, in the case of T(Niño 3), T(Niño) 4), and the SO index from [32], are analogous to Fig. 3 (not shown). The conclusion about the influence of ENSO on the NAO with the most likely delay of 24 months is drawn with a 0.95 confidence probability. No reverse influence is found. When T(Niño1+2) is used, even the ENSO effect on the NAO is not so evident: only $\hat{\gamma}_1 (\Delta = -21)$ is pointwise significant. The use of the anomalies of all indices instead of the indi-
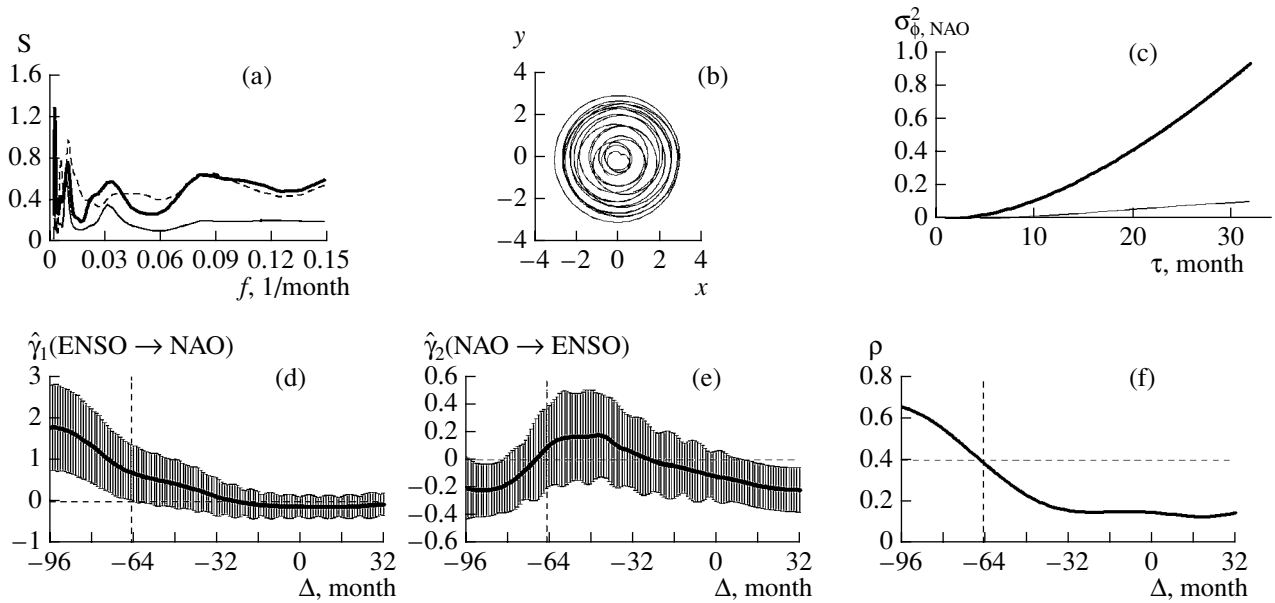
Fig. 5. Results of analysis analogous to those in Fig. 3, with the replacement of the NAO index from [32] by the NAO index from [31] for the 1950–2004 period: (a) global wavelet spectra (the thick line is the NAO index [31] for 1950–2004, the dashed line is the NAO index from [31] for 1871–2004, and the thin line is the reconstruction of the spectrum shown in Fig. 1 for the NAO index [32] for 1950–2004); (b) trajectory on a complex plane for $s = 32$ months (analogous to Fig. 1e); (c) dependence of the residual error of phase-dynamics model (6) on the parameter τ for the NAO index [31] (thick line), the error for the NAO from [32] in Fig. 3a is shown for comparison (thin line); (d–f) the same as in Figs. 3d–3f.

ces results in no change because the anomalies in the given frequency band do not differ from the indices themselves. For other rhythms of the NAO and ENSO, no mutual influence was detected in any of the cases.

A similar analysis was performed with data from [31] (1821–2004) for the NAO index, defined as the normalized pressure difference between two points in the North Atlantic, which is not as large-scale a characteristic as the NAO index from [32]. The length of this series is sufficient to analyze the coupling between the NAO and T(Niño3) for the 1971–1997 period, the NAO and SO for 1866–2004, and the NAO from [31] with the above ENSO indices from [32] for 1950–2004. Figure 5 shows results of coupling analysis for the NAO index from [31] and T(Niño3.4) from [32] for the 1950–2004 period. The width of the peak at the frequency corresponding to a 32-month scale is larger in the NAO spectrum from [31] than in the NAO spectrum from [32], even for the same 1950–2004 period (thick and thin lines in Fig. 5a). The trajectory on the complex plane (Fig. 5b) runs rather close to the origin of coordinates. These two facts indicate that phase diffusion for the selected NAO rhythm may be much greater when the data from [31] are used. This supposition confirmed by Fig. 5c, where it can be seen that the diffusion coefficient is an order of magnitude greater (the thick line against the thin line); i.e., it is on the same order of magnitude as that for the ENSO indices. As a consequence, no coupling is detected between the NAO and ENSO processes (Figs. 5d–5f). Analysis

of coupling of the NAO from [31] with the other ENSO indices for the 1950–2004 period gives similar results.

When the length of time series of the indices of the NAO [31], SO [31, 32], and T(Niño3) [19, 28, 70] is increased (i.e., the start of the analyzed time series is moved to the past), the shape of the power spectrum of the NAO index changes: the peak corresponding to a 32-month rhythm broadens and, finally, decays entirely (see the dashed line in Fig. 5a for the 1871–2004 period). Analysis was made of a greater number of NAO, SO, and T(Niño3) rhythms, such as a rhythm with a characteristic 60-month period and others, but none of them manifested a significant influence of the NAO on ENSO and vice versa. The influence of ENSO on the NAO was not found even for a 32-month rhythm nor was it found for a shorter fragment of the series (1950–2004). Thus, even the increase in the time series length does not provide a more reliable detection of coupling, because the noise level in the phase dynamics of the NAO from [31] is considerably higher.

Quantitative estimates of changes in the character of interaction of the ENSO and NAO processes are of particular interest. For this purpose, a special analysis was performed for the NAO and T(Niño3.4) indices [32] in a 47-yr moving time window during previous decades (1950–2004). Coupling estimates of a 32-month rhythm were obtained for nine positions of the window (with a 1-yr shift): beginning in 1950–1996 and ending in 1958–2004. The results for all the analyzed intervals were found to be analogous
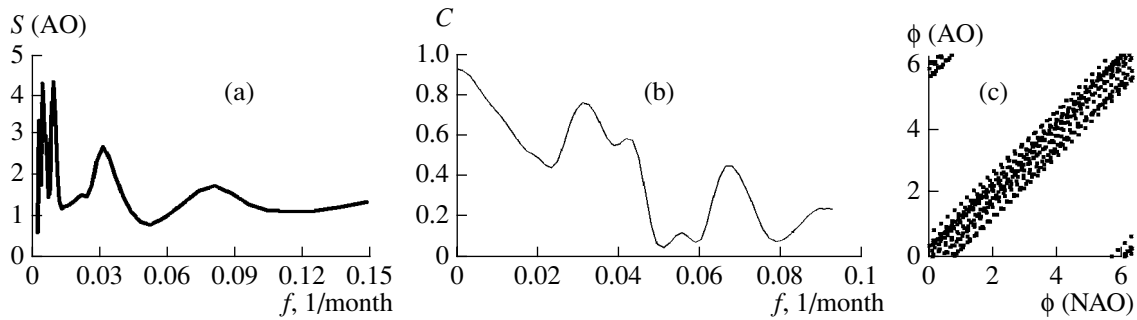
Fig. 6. Characteristics of the AO index and comparison with the NAO index [32] for 1950–2004: (a) global wavelet spectrum of the AO, (b) coherence function of the AO and NAO calculated by means of smoothing periodograms with a modified Bartlett window with $M = 100$ [71], (c) experimental points on the plane of wrapped phases of the NAO and AO for rhythms with $s = 32$ months.

to those in Figs. 3d and 3e and coincided with one another quantitatively within the estimation error. Therefore, no changes in the strength of the influence of ENSO on the NAO over recent years were detected with the phase-dynamics approach.

3.2. Analysis of Phase Dynamics of the ENSO and AO Processes

An appropriate analysis was carried out for the ENSO and AO indices. The AO index, like the NAO index from [32], is a more integral climatic characteristic than the NAO index from [31]. It characterizes variations in the field of sea-level pressure of the northern extratropics (north of 20° N). From analysis of the mutual influence of ENSO and AO processes, other results can be expected, although the NAO and AO are strongly correlated. The global wavelet spectrum of the NAO index from [32] for 1950–2004 is shown in Fig. 6a. The peak corresponding to a 32-month rhythm and some others, including the annual cycle, are distinguished. Figure 6b displays the coherence function for the NAO and AO indices from [32] for 1950–2004. It nearly reaches a value of 0.8 for a 32-month rhythm. The experimental points on the plane of wrapped phases of the NAO and AO indices for this rhythm (Fig. 6c) show that the oscillations are largely synchronous and occur in phase.
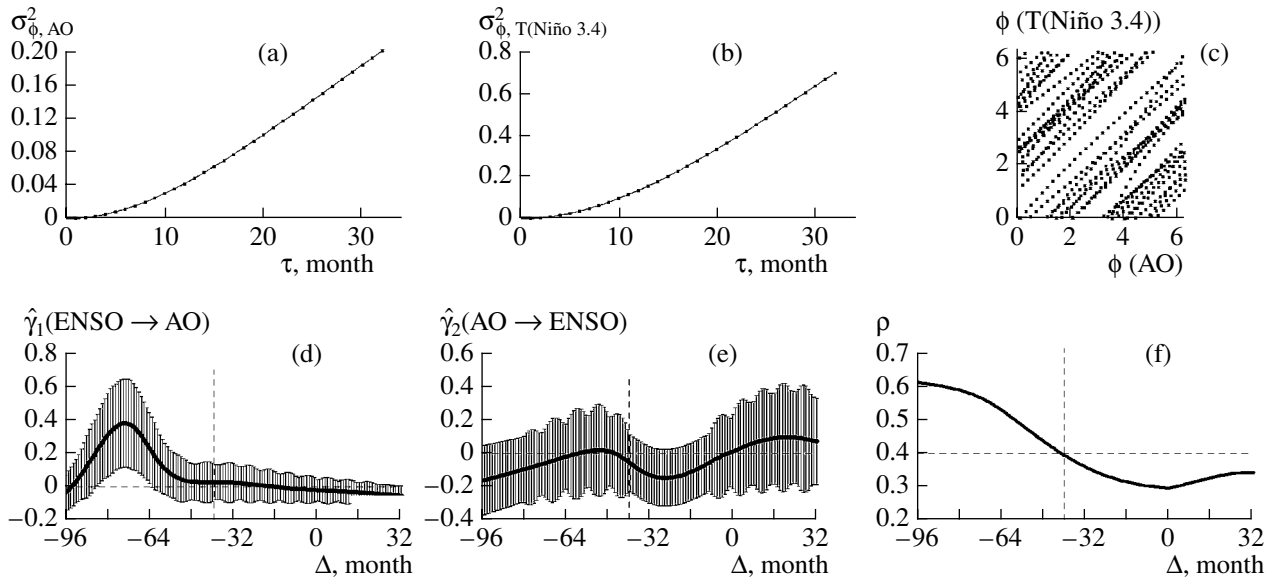
Results from analysis of coupling between the AO and El Niño (T(Niño3.40) from [32] (1950–2004) for a rhythm with $s = 32$ months are shown in Fig. 7. Phase diffusion for the AO index (Fig. 7a) is weaker than that for T(Niño 3.4) (Fig. 7b) but twice as strong as the phase diffusion for the NAO index (Fig. 3a). For $\Delta > -40$, there is no synchrony between oscillations (Figs. 7c, 7f) and the phase-dynamics approach is applicable. The coupling estimates shown in Figs. 7d and 7e suggest that no reliable conclusions can be inferred about the influence of the AO and ENSO on each other. Identical results were obtained for other rhythms and other ENSO indices (not shown). The absence of evident indications of the ENSO effect on the AO, despite the presence of the influence of the ENSO on the NAO, can be explained by the fact that the AO process is influenced by a larger number of factors (since it is more global). This leads to the enhancement of the effective noise in phase dynamics (as was noted in analysis of Figs. 3a and 7a). As a result, the detection of weak coupling from such a short series becomes difficult.

3.3. Prediction Models for the ENSO and NAO Processes

We performed the analysis of coupling, which takes into account not only the phases but also amplitudes of the signals with the use of cross-correlation functions and nonlinear prediction models. Results for the NAO index and T(Niño3.4) from [32] for 1950–2004 are shown in Fig. 8. Negative shift values for the cross-correlation function (CCF) in Fig. 8a correspond to the situation where T(Niño3.4) leads. The CCF is "almost" pointwise significant at the level $p < 0.05$ for $\Delta = -20$ and $\Delta = -82$ months, but no general confident inference about nonzero correlation between the analyzed processes can be made.

More realistic results were obtained via construction of prediction models. Figures 8b and 8c show $PI_{2 \to 1}$ and $PI_{1 \to 2}$ for models (11) with $d_1 = 0, d_2 = 1$, and $K = 2$. The prediction of the NAO is improved by 1.5 to 2% via incorporation of the El Niño (T(Niño3.4)) with $\Delta = -(19–21)$ and $\Delta = -(80–83)$ months. This result corresponds to the above delays for the CCF. Each of these values is significant according to an F-test at the level $p < 0.01$. Taking into account strong correlations of $PI_{2 \to 1}$ separated in Δ by an interval not greater than 4 and considering arguments analogous to those in Section 3.1, one can draw a general inference about the presence of the influence of El Niño on the NAO from [32] even for one of the indicated Δ values with a confidence probability of at least 0.95. The values $\Delta = -(19–21)$ are roughly consistent with the results of phase-dynamics modeling,

Fig. 7. Analysis of coupling between the AO and T(Niño3.4) (from [32] for 1950–2004) by the method of phase-dynamics modeling for rhythms with $s = 32$ months. Notations are the same as in Fig. 3.

so that it is possibly these values that adequately characterize the time delay in the ENSO effect on the NAO. It is not improbable that both groups of Δ correspond to a real delayed influence of ENSO on the NAO.

There is also an improvement of 1–2% in the prediction of T(Niño3.4) achieved via considerstion of the NAO with $\Delta = -(48–49)$ months, which is individually significant at the level $p < 0.01$. However, it does not allow the confident conclusion that the NAO affects ENSO. It is only a weak (unreliable) indication of an effect. However, if this indication is taken into consideration, one can note that the sum of delays in the influence of ENSO on the NAO (about 20 months) and the NAO on ENSO (30 to 50 months) is 50 to 70 months. The rhythm with a typical oscillation period of some 60 months is well pronounced in the dynamics of ENSO indices. This rhythm can be assumed to result from a mutual delayed coupling between the ENSO and NAO processes. This is not a reliable inference, but an assumption, and it is unclear why the same rhythm is not manifested in the dynamics of the NAO.

The inferences made above have been obtained via the simplest models, in which their own dynamics (dependence of the current value of a variable on its past values) was disregarded. Granger causality requires that the improvement of the prediction be achieved only by incorporation of a variable of the other system, not by complication of an individual model. When d_1 (dimension of an individual model) is changed to 2 inclusive, the results actually remain unchanged (not shown). This confirms their significance. If d_1, the polynomial order, and d_2 are simulta-

neously increased to 3, 3, and 2, respectively, no reliable inferences about coupling can be drawn, because of the broadening of confidence intervals. The explanation for this circumstance is that the number of estimated parameters in such a complicated model grows to 56 and, with the length of the time series being constant, the variance of estimates increases. Therefore, for relatively short series, we have to restrict ourselves to the results presented for the most "compact" models.

An analogous analysis of coupling for the NAO indices and T(Niño3.4) anomalies from [32] yields plots qualitatively similar to those in Figs. 8b and 8c (not shown), but the inference about the ENSO effect on the NAO is drawn with somewhat less reliability, at the level $p < 0.1$. In regard to the reverse influence of the NAO on ENSO, only its weak indications can be discerned, as in the case with the T(Niño3.4) index itself. Identical results are obtained if T(Niño3) (or its anomalies), T(Niño4) (or its anomalies), or the SO index is used instead of the T(Niño3.4) anomaly. If the T(Niño1+2) index is used, the conclusions are even less significant.

Analogously to the results of phase-dynamics modeling (Section 3.1), with the use of the NAO index from [31] instead of the NAO index from [32], no significant influence of ENSO on the NAO was detected either for the period 1950–2004 or for other periods since the 19th century. Consequently, the inferences based on the two methods using different NAO and ENSO indices are well consistent, so that the confidence in the results obtained increases.

Examination of changes in the character of coupling [32] for the NAO index and T(Niño3.4) in a moving time window during 1950–2004 (see the end
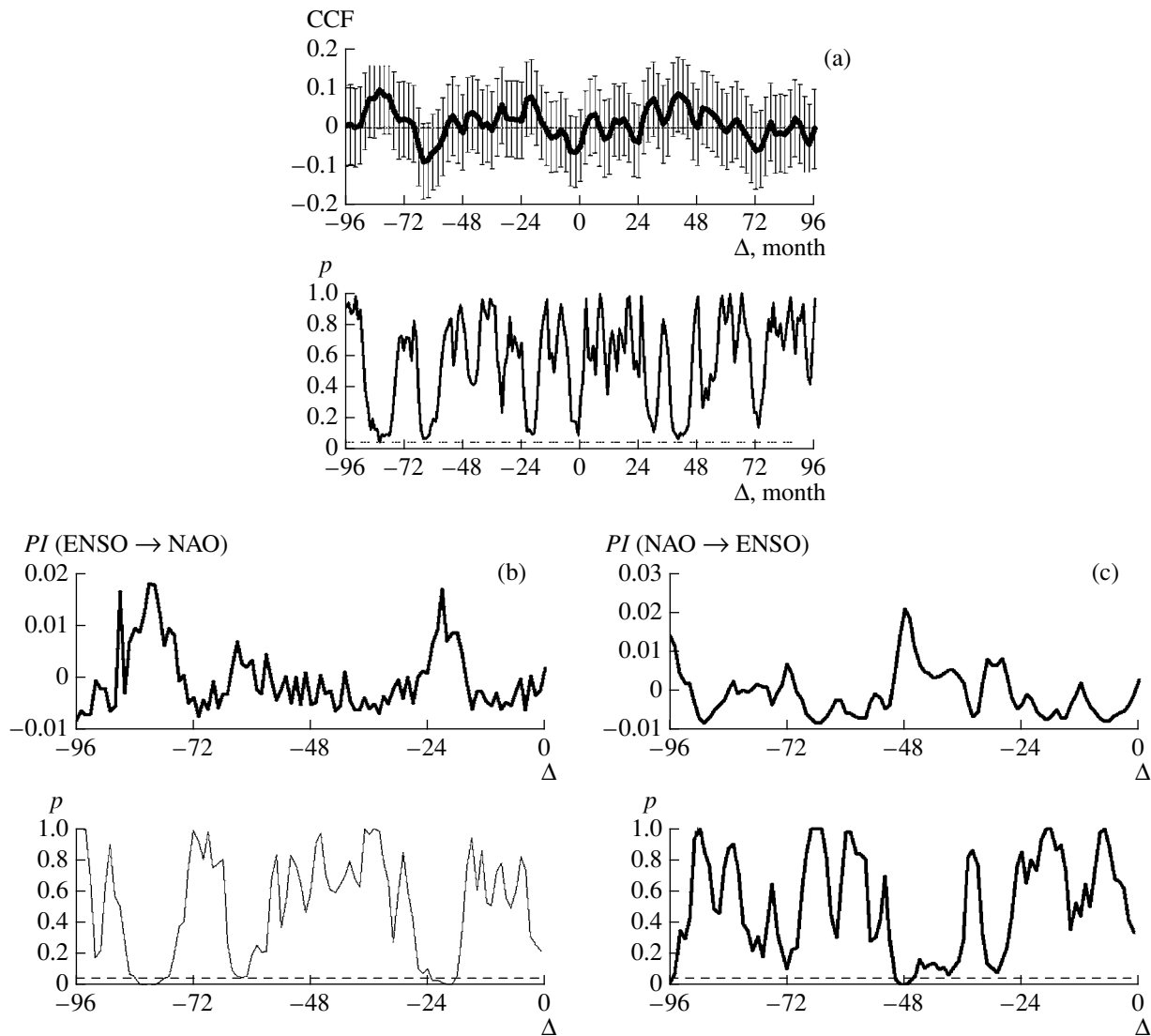
Fig. 8. Analysis of coupling between the NAO index and T(Niño 3.4) (from [32] for 1950–2004) with the use of correlation functions and prediction models: (a) cross-correlation function, 95% confidence interval with a halfwidth equal to a double error estimate from the Bartlett formula under the assumption that the processes are uncorrelated [71], and the significance level is calculated under the assumption of normally distributed estimate values; and (b, c) improvement of the prediction of the NAO with consideration for T(Niño3.4) and vice versa. The dashed line represents the level $p = 0.05$.

of Section 3.1) revealed a strengthening of the ENSO effect on the NAO over recent years. Qualitatively, the plots of the prediction-error improvement and the model coefficients are analogous to Figs. 8b and 8c. However, $PI_{2 \to 1}$ (the improvement of the prediction of the NAO when the ENSO is taken into account) for $\Delta = -(19–20)$ months increases almost monotonically by about a factor of 2.5 with a shift of the time interval (from 1950–1996 to 1958–2004) (Fig. 9). Nearly identical results are obtained for $\Delta = -81$ months.

Although the statistical significance of the inference about the increase in $PI_{2 \to 1}$ is hard to estimate, the monotone pattern of this increase indicates that it does not resemble the effect of random errors in statistical estimation. The oscillation amplitude (standard deviation) of the NAO index from [32] in a moving time interval fluctuates within 1% when the interval is shifted. The amplitude of T(Niño3.4) systematically grows (by about 7%), with a peak in the 1955–2001 window, and then decreases slightly. Increasing the amplitude of ENSO, with an interaction held constant, could have led to an increase in $PI_{2 \to 1}$. However, it is possible to show that a 7% increase in x_2 in model (11) with $d_1 = 0$, $d_2 = 1$, and $K = 2$ may cause $PI_{2 \to 1}$ to grow by no more than 20%. Therefore, the improvement of the prediction of the NAO by a factor of 2.5 when the ENSO is taken into account cannot be explained solely by a change in the ENSO amplitude.
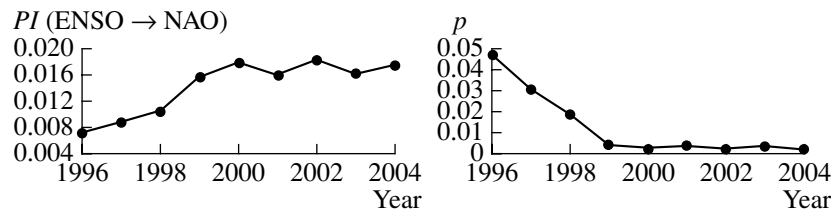
Fig. 9. Improvement of the prediction error of the NAO [32] with consideration for T(Niño3.4) (maximum of the values corresponding to delays of –19 and –20 months) and its pointwise significance level as a function of the position of a moving average (the end year of a time interval is plotted on the abscissa axis).

A conclusion is to be made about the recent increase in the ENSO effect on the NAO. This phenomenon is precisely due to the strengthening over recent years, not the weakening of the 1950–1958 period, because the coupling is more clearly defined for the whole 1950–2004 period than for 1950–1996.

As far as changes in the NAO effect on the ENSO are concerned, it is hard to say anything about them because even the presence of this effect cannot be reliably detected.

3.4. Prediction Models for the ENSO and AO

Analysis of the mutual influence of the ENSO and AO processes with different indices was performed in a similar way. The results obtained for the AO index and T(Niño 3.4) anomalies from [32] for 1950–2004 indicate that the presence of influence in either direction cannot be reliably detected, although pointwise significant coefficients are obtained for roughly the same delays as in the case with the NAO (not shown). The most reliable conclusion to be inferred from this analysis is the existence of a negative cross correlation between the AO index and T(Niño3.4) with a 1-month delay, when ENSO leads. This correlation is pointwise significant at the level $p < 0.02$, but no reliable general inference about coupling can be made. Similar results were obtained for other temperature ENSO indices.

3.5. Analysis of Winter ENSO, NAO, and AO Regimes

The NAO, AO, and ENSO are most evident during the NH winter. For this reason, an additional analysis was performed for the NH winter seasons, from December through February. The corresponding time series of the winter means of the indices are 12 times shorter than the original time series of the monthly means. Results of the estimation of cross-correlation functions are shown in Fig. 10.

The CCF of the NAO index and T(Niño3.4) is pointwise significant at the level $p < 0.05$ for delays of –1 year, –3 years, and –8 years (ENSO leads, see Fig. 10a). No reliable general conclusion about non-zero correlation can be made.

For the NAO index and T(Niño3), the correlation is pointwise significant if $p < 0.0025$ for a delay of −1 year (Fig. 10b). Then, by multiplying the pointwise significance level by 21 (the total number of the shifts considered), one can infer a general conclusion about nonzero correlation for a significance level $p < 0.05$.

For the NAO index and T(Niño4), the correlation is pointwise significant if $p < 0.05$ with a delay of −3 years (ENSO leads, see Fig. 10c). No reliable general conclusion can be made.

For the NAO index and T(Niño1+2), the correlation is pointwise significant if $p < 0.001$ with a delay of –1 year (Fig. 10d). One can draw a general conclusion about nonzero correlation for a significance level of $p < 0.02$.

For the NAO and SO indices taken from [32] for the 1950–2004 period, the correlation is pointwise significant with delays of –2 years and –8 years (correlation coefficient is negative) (Fig. 10e). No reliable general inference can be drawn.

For the NAO index from [31] and T(Niño3) in the analysis of their longer series (1871–1979), there is only a pointwise significant correlation for $p < 0.05$ with a delay of –1 year. A reliable conclusion about coupling cannot be made either, nor can it be made with the use of other methods for analysis of longer series.

The nonlinear prediction models provide no other results (or a more reliable support of the same results).

On the whole in all cases of mutual dynamics of the ENSO and NAO, a significant correlation is reliably detected for the NH winter seasons (for shorter T(Niño3) and T(Niño1+2) series), when the ENSO drives NAO. The opposite situation (when the NAO drives ENSO) is not detected. Thus, the inference about the ENSO effect on the NAO is confirmed by the winter mean values of the indices, with a time delay being estimated at 1 to 3 years.

For the CCF of the AO index and temperature ENSO indices, negative values of about –0.1 (insignificant) are obtained for a zero delay. For the AO index and any of the ENSO indices, no pointwise significant correlation is found for any time delay.
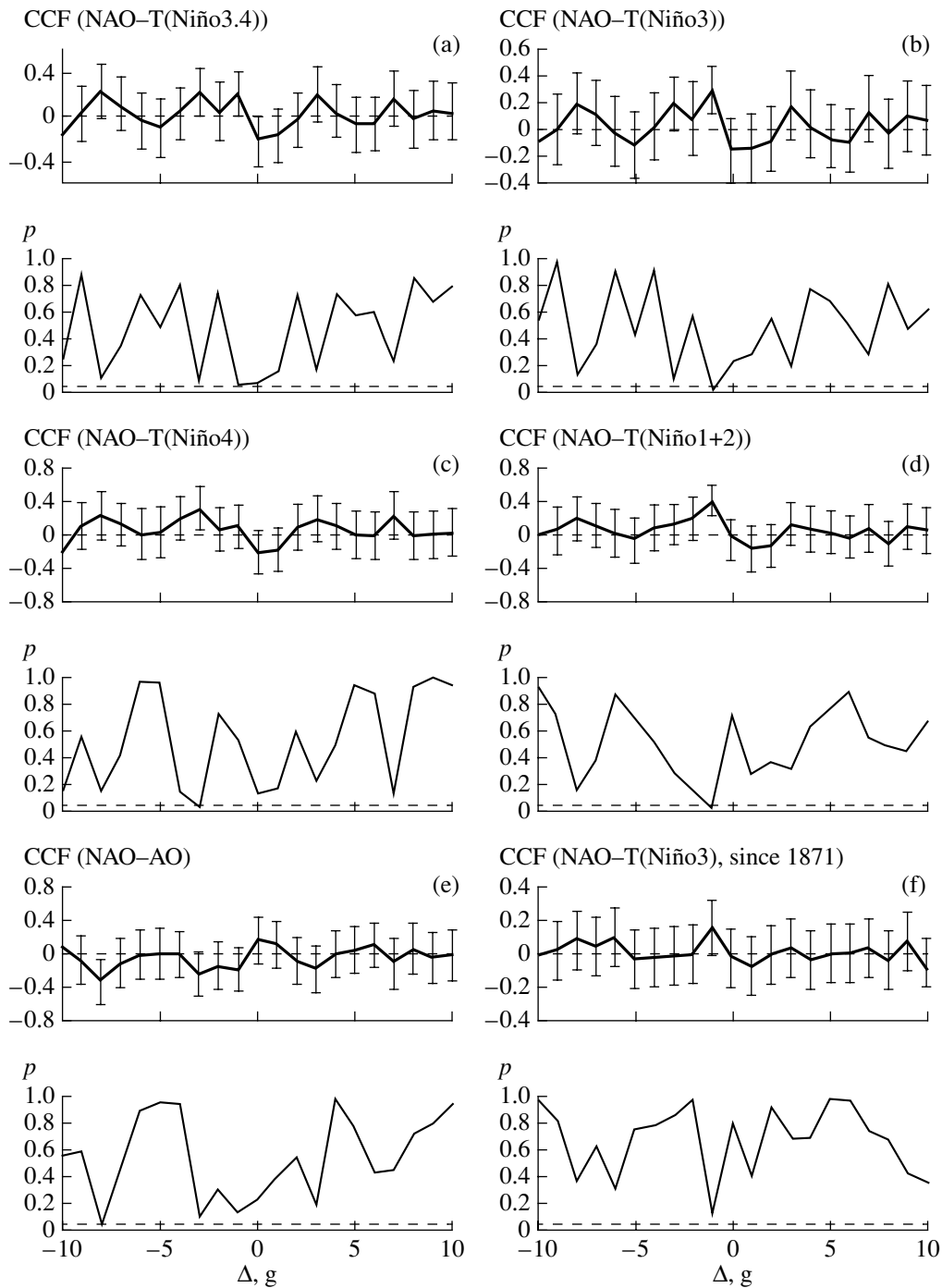
Fig. 10. Cross-correlation functions of the winter mean NAO and ENSO indices for 1950–2004 from [32]. In panel (e), the NAO for 1871–1997 from [31] is shown. Time shifts are in years. The 95% confidence interval is the same as in Fig. 8a.

Analysis of changes in cross correlations among all the indices from [32] for "46-winter" moving time intervals (see Sections 3.1, 3.3) during 1950–2004 reveals only fluctuations within 1–3%.

4. CONCLUSIONS

From the analysis performed with different linear and nonlinear methods (including the phase-dynamics approach, nonlinear prediction models, and estimation of cross-correlation functions), a number of features of the interdependence of ENSO, NAO, and AO events were detected with the use of various climatic indices characterizing these climatic cycles. In all cases, the results were shown to be consistent with one another.

The ENSO effect on the NAO from [32] during the 1950–2004 period was detected with a confidence

probability of at least 0.95–0.98 for the following cases:

(i) the phase-dynamics approach with a confidence probability of at least 0.95 for the NAO and ENSO indices (T(Niño3.4), T(Niño3), T(Niño4, and the AO index) in the frequency band corresponding to time scales of 28–36 months;

(ii) construction of nonlinear prediction models for the NAO and ENSO indices with a confidence probability of at least 0.95 for T(Niño3.4) and 0.9 for T(Niño3), T(Niño4), and AO indices and all anomalies of these indices; and

(iii) correlation analysis of the winter mean (for the NH) NAO and ENSO indices with a confidence probability no lower than 0.98 for T(Niño1+2) and 0.95 for T(Niño3).

The time delay of the ENSO effect on the NAO from [32] is estimated at 1 to 3 years, with the most probable value of 20 to 24 months.

Analysis of longer time series (in particular, for the period 1871–1997) shows no ENSO effect on the NAO. This outcome is related to specific properties of the NAO index from [31], which is not as large-scale a characteristic as the NAO index from [32].

The analysis of data from [32] that is based on the prediction models has shown that there is a tendency for the influence of ENSO on the NAO to increase in recent years. The prediction of the NAO when the ENSO is taken into account (with a delay of 19 to 20 months) improves by a factor of 2–2.5; however, the reliability of this inference is difficult to estimate.

Note that a qualitative evolution of climate variability and predictability may be associated with a strengthening of the coupling between the NAO and the ENSO and, in general, with a change of the oscillatory properties of the Earth's climate system (ECS). In [72, 73], for example, from global surface temperature data over a hundred years from the late 19th century to the late 20th century, it is shown that the 4- to 6-year cycles, which are typical of El Niño events and to which the strongest variations in interannual variability are interrelated, have a tendency to decrease during global warming. It is also shown that resonance properties of the ECS (including parametric resonance) may substantially change in the case of occurrence of a similar tendency during a global warming of about 1 K.

The opposite influence of the NAO on ENSO is not detected with confidence. There are only weak indications for such an effect with a delay of 30 to 50 months in the data of [32]. If this influence takes place, the sum of delays of the ENSO relative to the NAO and of the NAO relative to the ENSO is close to the length of a typical 60-month cycle in ENSO dynamics. This indicates that the presence of such a cycle can be interpreted as a manifestation of the corresponding delayed feedback.

The interaction of the AO with ENSO is not found with reliability. Only a negative value of the cross-correlation function with a zero delay or a delay of −1 month (ENSO leads AO) is found, but the inference is not confident.

Overall in this study, the delay in the influence of the ENSO process on the NAO in recent decades is detected with a high degree of reliability. The results depend heavily on the choice of the NAO index and on the technique of analysis.

ACKNOWLEDGMENTS

APPENDIX A

COUPLING ESTIMATORS
IN THE PHASE-DYNAMICS APPROACH

Formulas for coupling estimators $\hat{\gamma}_{1,2}$ are derived for a system of linear uncoupled oscillators with normal white noise [53] and are expressed through coefficient estimates (3), where the functions F_i are trigonometric polynomials

$$F_i = \sum_{m,n} [a_{i,m,n}\cos(m\phi_1 + n\phi_2) \quad \text{(A1)}$$
$$+ b_{i,m,n}\sin(m\phi_1 + n\phi_2)], \quad i = 1, 2,$$

and $\mathbf{a}_i = \{a_{i,m,n}, b_{i,m,n}\}_{m,n}$, $i = 1, 2$, are vectors of their coefficients. The coefficients of polynomials $\hat{a}_{i,m,n}$ and $\hat{b}_{i,m,n}$ are estimated with the LSM (4), and estimates of their variances are expressed as

$$\hat{\sigma}^2_{\hat{a}_{i,m,n}} = \frac{2\hat{\sigma}^2_{\varepsilon_i}}{N-k}\left(1 + 2\sum_{l=1}^{k-1}\left(1 - \frac{l}{k}\right)\right.$$
$$\left. \times \cos\left(\frac{l(m\hat{a}_{1,0,0} + n\hat{a}_{2,0,0})}{k}\right)\exp\left(-\frac{l(m^2\hat{\sigma}^2_{\varepsilon_1} + n^2\hat{\sigma}^2_{\varepsilon_2})}{2k}\right)\right), \quad \text{(A2)}$$

where $\hat{\sigma}^2_{\varepsilon_i}$ is the estimate of the variance of the noise ε_i in difference equations (3)

$$\hat{\sigma}^2_{\varepsilon_i} = \frac{1}{N-k-L_i}\sum_{j=1}^{N-k}\left(\Delta_i(t_j) - \frac{1}{N-k}\sum_{l=1}^{N-k}\Delta_i(t_l)\right)^2, \quad \text{(A3)}$$

with L_i being the number of coefficients of the polynomial F_i. For the variances $\hat{b}_{l, m, n}$, the expression is analogous.

An expression for $\hat{\gamma}_1$ in terms of estimates of the coefficients and their variances is

$$\hat{\gamma}_1 = \sum_{m, n} n^2(\hat{a}_{1, m, n}^2 + \hat{b}_{1, m, n}^2 - 2\hat{\sigma}_{\hat{a}_{1, m, n}}^2). \qquad (A4)$$

An expression for $\hat{\gamma}_2$ is written analogously. The estimate of the variance of $\hat{\gamma}_1$ is written as

$$\hat{\sigma}_{\hat{\gamma}_1}^2 = \begin{cases} \sum_{m, n} n^4(\hat{\sigma}_{\hat{a}_{1, m, n}^2}^2 + \hat{\sigma}_{\hat{b}_{1, m, n}^2}^2), \text{ if} \\ \hat{\gamma}_1 \geq 5\sqrt{\sum_{m, n} n^4(\hat{\sigma}_{\hat{a}_{1, m, n}^2}^2 + \hat{\sigma}_{\hat{b}_{1, m, n}^2}^2)} \\ \frac{1}{2}\sum_{m, n} n^4(\hat{\sigma}_{\hat{a}_{1, m, n}^2}^2 + \hat{\sigma}_{\hat{b}_{1, m, n}^2}^2), \end{cases} \qquad (A5)$$

where

$$\hat{\sigma}_{\hat{a}_{i, m, n}}^2 = \begin{cases} 2\hat{\sigma}_{\hat{a}_{i, m, n}}^4 + 4(\hat{a}_{i, m, n}^2 - \hat{\sigma}_{\hat{a}_{i, m, n}}^2)\hat{\sigma}_{\hat{a}_{i, m, n}}^2, \text{ if} \\ \hat{a}_{i, m, n}^2 - \hat{\sigma}_{\hat{a}_{i, m, n}}^2 \geq 0 \\ 2\hat{\sigma}_{\hat{a}_{i, m, n}^2}^4, \end{cases} \qquad (A6)$$

with a similar expression for $\hat{\sigma}_{\hat{b}_{i, m, n}^2}^2$ and calculation of the estimate of the variance of $\hat{\gamma}_2$.

Confidence intervals for coupling estimators are expressed in terms of their variances. For example, a 95% confidence interval was found semiempirically and is written as $[\hat{\gamma}_i - 1.6\hat{\sigma}_{\hat{\gamma}_i}, \hat{\gamma}_i + 1.8\hat{\sigma}_{\hat{\gamma}_i}]$ for $\hat{\gamma}_i$. The conclusion about the influence of system 2 on system 1 is made for $\hat{\gamma}_1 - 1.6\hat{\sigma}_{\hat{\gamma}_1} > 0$. Likewise, the influence of system 1 on system 2 is manifested if $\hat{\gamma}_2 - 1.6\hat{\sigma}_{\hat{\gamma}_2} > 0$. The probability of a random error in either of these cases (i.e., the inference about connection of uncoupled systems) is 0.025 because only erroneously positive values of estimates are "dangerous."

REFERENCES

1. *CLIVAR Initial Implementation Plan*, WCRP, No. 103; WMO/TD, No. 869; ICPO, No. 14 (1998); http://www.clivar.dkrz.de/hp.html.

2. *Climate Change 2001: The Scientific Basis. Intergovernmental Panel on Climate Change*, Ed. by J. T. Houghton, Y. Ding, D. J. Griggs, M. Noguer, et al. (Cambridge Univ. Press, Cambridge, 2001).

3. J. Bjerknes, "Atmospheric Teleconnections from the Equatorial Pacific," Mon. Weather Rev. **97**, 163–172 (1969).

4. J. M. Wallace and D. S. Gutzler, "Teleconnections in the Geopotential Height Field During the Northern Hemisphere Winter," Mon. Weather Rev. **109**, 784–812 (1981).

5. J. C. Rogers, "The Association between the North Atlantic Oscillation and the Southern Oscillation in the North Hemisphere," Mon. Weather Rev. **112**, 1999–2015 (1984).

6. J. W. Hurrell, "Decadal Trends in the North Atlantic Oscillation: Regional Temperatures and Precipitation," Science **269** (1995).

7. J. W. Hurrell and H. van Loon, "Decadal Variations Associated with the North Atlantic Oscillation," Clim. Change **36**, 301–326 (1997).

8. J. M. Wallace, "North Atlantic Oscillation/Northern Hemisphere Annual Mode: Two Paradigms—One Phenomenon," Q. J. R. Meteorol. Soc. **126** (2000).

9. A. G. Barnston and R. E. Livezey, "Classification, Seasonality, and Persistence of Low Frequency Atmospheric Circulation Patterns," Mon. Weather Rev. **115**, 1083–1126 (1987).

10. I. I. Mokhov and V. K. Petoukhov, *Spatiotemporal Climatic Structures, Parts I, II* (IFA AN SSSR, Moscow, 1989) [in Russian].

11. S. G. H. Philander, *El Niño La Niña and the Southern Oscillation* (Academic, London, 1990).

12. *The TOGA decade: Reviewing the Progress of El Niño Research and Prediction*, Ed. by D.L.T. Anderson, E. S. Sarachik, P. J. Webster, and L. M. Rothstein, J. Geophys. Res. C, **103**, 14167–14510 (1998).

13. D. Yu. Gushchina and M. A. Petrosyants, "Relationship between the Sea Surface Temperature in the Equatorial Pacific and the Wind-Velocity Circulation at the Centers of Atmospheric Action," Meteorol. Gidrol., No. 12, 5–22 (1998).

14. N. A. Dianskii, "Spatiotemporal Patterns between the Coupled Modes of 500-mb Geopotential Height and Sea Surface Temperature Anomalies in the Wintertime North Atlantic," Izv. Akad. Nauk, Fiz. Atm. Okeana **34**, 197–213 (1998) [Izv., Atmos. Ocean. Phys. **34**, 176–190 (1998)].

15. H. Von Storch and F. W. Zwiers, *Statistical Analysis in Climate Research* (Cambridge Univ. Press, Cambridge, 1999).

16. K. Arpe, L. Bengtsson, G. S. Golitsyn, et al., "Analysis and Modeling of Change in the Hydrologic Cycle in the Caspian Basin," Dokl. Akad. Nauk **366**, 248–252 (1999).

17. K. Arpe, L. Bengtsson, G. S. Golitsyn, et al., "Connections between Caspian Sea Level Variability and ENSO," Geophys. Rev. Lett. **27**, 2693–2696 (2000).

18. I. I. Mokhov, A. V. Eliseev, D. Handorf, et al., "North Atlantic Oscillation: Diagnosis and Simulation of Decadal Variability and Its Long-Period Evolution," Izv. Akad. Nauk, Fiz. Atmos. Okeana **36**, 605–616 (2000) [Izv., Atmos. Ocean. Phys. **36**, 555–565 (2000)].

19. I. I. Mokhov, A. V. Eliseev, and D. V. Khvorost'yanov, "Evolution of the Characteristics of Interannual Climate Variability Associated with the El Niño and La Niña Phenomena," Izv. Akad. Nauk, Fiz. Atmos. Okeana **36**,

741–751 (2000) [Izv., Atmos. Ocean. Phys. **36**, 681–690 (2000)].

20. C. Deser, "On the Teleconnectivity of the Arctic Oscillation," Geophys. Rev. Lett. **27**, 779–782 (2000).

21. V. A. Bezverkhnii, "Developing the Wavelet-Transform Method for Analysis of Geophysical Data," Izv. Akad. Nauk, Fiz. Atmos. Okeana **37**, 630–638 (2001) [Izv., Atmos. Ocean. Phys. **37**, 584–591 (2001)].

22. H. Wanner, S. Bronnimann, and C. Casty, "North Atlantic Oscillation—Concepts and Studies," Surv. Geophys. **22**, 321–382 (2001).

23. D. Pozo-Vazquez, M. J. Esteban-Parra, F. S. Rodrigo, and Y. Castro-Diez, "The Association between ENSO and Winter Atmospheric Circulation and Temperature in the North Atlantic Region," J. Clim. **14**, 3408–3420 (2001).

24. A. B. Polonsky and D. V. Basharin, "On the Influence of the North Atlantic and Southern Oscillations on the Variability of Air Temperature in the Mediterranean-European Region," Izv. Akad. Nauk, Fiz. Atmos. Okeana **38**, 135–145 (2002) [Izv., Atmos. Ocean. Phys. **38**, 119–128 (2002)].

25. U. Merkel and M. Latif, "A High Resolution AGCM Study of the El Niño Impact on the North Atlantic/European Sector," Geophys. Rev. Lett. **29**, 1291, doi: 10.1029/2001GL013726 (2002).

26. H. Lin, J. Derome, R. J. Greatbath, et al., "Tropical Links of the Arctic Oscillation," Geophys. Rev. Lett. **29**, 1943, doi: 10.1029/2002GL015822 (2002).

27. S. Jevrejeva, J. Moore, and A. Grinsted, "Influence of the Arctic Oscillation and El Niño–Southern Oscillation (ENSO) on Ice Conditions in the Baltic Sea: The Wavelet Approach," J. Geophys. Res. **108**, 4677, doi: 10.1029/2003JD003417 (2003).

28. I. I. Mokhov, D. V. Khvorostyanov, and A. V. Eliseev, "Decadal and Longer Term Changes in El Niño—Southern Oscillation Characteristics," Int. J. Climatol. **24**, 401–414 (2004).

29. A. Grinsted, J. C. Moore, and S. Jevrejeva, "Application of the Cross Wavelet Transform and Wavelet Coherence to Geophysical Time Series," Nonlin. Proc. Geophys. **11**, 561–566 (2004).

30. I. I. Mokhov, V. A. Bezverkhny, and A. A. Karpenko, "Diagnosis of Relative Variations in Atmospheric Greenhouse Gas Contents and Temperature from Vostok Antarctic Ice-Core Paleoreconstructions," Izv. Akad. Nauk, Fiz. Atmos. Okeana **41**, 579–592 (2005) [Izv., Atmos. Ocean. Phys. **41**, 523–536 (2005)].

31. URL: http://www.cru.uea.ac.uk.

32. URL: http://www.ncep.noaa.gov.

33. Quian Quiroga R., A. Kraskov, T. Kreuz, and P. Grassberger, "Performance of Different Synchronization Measures in Real Data: A Case Study on Electroencephalographic Signals," Phys. Rev. E **65**, 041903 (2002).

34. D. A. Smirnov and R. G. Andrzejak, "Detection of Weak Directional Coupling: Phase-Dynamics Approach versus State-Space Approach," Phys. Rev. E **71**, 036207 (2005).

35. A. Cenys, G. Lasiene, and K. Pyragas, "Estimation of Interrelation between Chaotic Observables," Phys. D (Amsterdam) **52**, 332–337 (1991).

36. N. F. Rulkov, M. M. Sushchik, L. S. Tsimring, and H. D. I. Abarbanel, "Generalized Synchronization of Chaos in Directionally Coupled Chaotic Systems," Phys. Rev. E **51**, 980–994 (1995).

37. S. J. Schiff, P. So, T. Chang, et al., "Detecting Dynamical Interdependence and Generalized Synchrony through Mutual Prediction in a Neural Ensemble," Phys. Rev. E **54**, 6708–6724 (1996).

38. J. Arnhold, K. Lehnertz, P. Grassberger, and C. E. Elger, "A Robust Method for Detecting Interdependences: Application to Intracranially Recorded EEG," Phys. D (Amsterdam) **134**, 419–430 (1999).

39. M. Le Van Quyen, J. Martinerie, C. Adam, and F. Varela, "Nonlinear Analyses of Interictal EEG Map the Brain Interdependences in Human Focal Epilepsy," Phys. D (Amsterdam) **127**, 250–266 (1999).

40. T. Schreiber, "Measuring Information Transfer," Phys. Rev. Lett. **85**, 461–464 (2000).

41. M. Palus, V. Komarek, Z. Hrncir, and K. Sterbova, "Synchronization As Adjustment of Information Rates: Detection from Bivariate Time Series," Phys. Rev. E **63**, 046211 (2001).

42. U. Feldmann and J. Bhattacharya, "Predictability Improvement As an Asymmetrical Measure of Interdependence in Bivariate Time Series," Int. J. Bifurc. Chaos **14**, 505–514 (2004).

43. R. F. Galan, R. Ritz, P. Szyszka, and A. V. M. Herz, "Uncovering Short-Time Correlations between Multichannel Recordings of Brain Activity: A Phase-Space Approach," Int. J. Bifurc. Chaos **14**, 585–597 (2004).

44. N. Ancona, D. Marinazzo, and S. Stramaglia, "Radial Basis Function Approach to Nonlinear Granger Causality of Time Series," Phys. Rev. E **70**, 056221 (2004).

45. T. Kiemel and A. H. Cohen, "Estimation of Coupling Strength in Regenerated Lamprey Spinal Cords Based on a Stochastic Phase Model," J. Comput. Neurosci. **5**, 267–284 (1998).

46. F. Mormann, K. Lehnertz, P. David, and C. E. Elger, "Mean Phase Coherence As a Measure for Phase Synchronization and Its Application to the EEG of Epilepsy Patients," Phys. D (Amsterdam) **144**, 358–369 (2000).

47. A. S. Pikovsky, M. G. Rosenblum, and J. Kurths, "Phase Synchronization in Regular and Chaotic Systems," Int. J. Bifurc. Chaos **10**, 2291–2305 (2000).

48. M. G. Rosenblum, A. S. Pikovsky, J. Kurths, et al., "Phase Synchronization: From Theory to Data Analysis," in *Neuro-Informatics, Handbook of Biological Physics*, Vol. 4, Ed. by F. Moss and S. Gielen (Elsevier Science, New York, 2001).

49. M. G. Rosenblum and A. S. Pikovsky, "Detecting Direction of Coupling in Interacting Oscillators," Phys. Rev. E **64**, 045202 (2001).

50. M. G. Rosenblum, L. Cimponeriu, A. Bezerianos, et al., "Identification of Coupling Direction: Application to Cardiorespiratory Interaction," Phys. Rev. E **65**, 041909 (2002).

51. M. Palus and A. Stefanovska, "Direction of Coupling from Phases of Interacting Oscillators: An Information-Theoretic Approach," Phys. Rev. E **67**, 055201 (2003).

52. T. Kiemel, K. M. Gormley, L. Guan, et al., "Estimating the Strength and Direction of Functional Coupling in the

Lamprey Spinal Cord," J. Comput. Neurosci. **15**, 233–245 (2003).

53. D. A. Smirnov and B. P. Bezruchko, "Estimation of Interaction Strength and Direction from Short and Noisy Time Series," Phys. Rev. **68**, 046209 (2003).

54. I. I. Mokhov and D. A. Smirnov, "El Niño Southern Oscillation Drives North Atlantic Oscillation As Revealed with Nonlinear Techniques from Climatic Indices," Geophys. Rev. Lett. **33**, EL03708. doi: 1029/2005GL024557 (2006).

55. D. Gabor, "Theory of Communication," J. IEEE (London), **93**, 429–459 (1946).

56. N. E. Huang, Z. Shen, and S. R. Long, "The Empirical Mode Decomposition and the Hilbert Spectrum for Nonlinear and Non-Stationary Time Series Analysis," Proc. R. Soc. London, Ser. A **454**, 903–995 (1998).

57. J. P. Lachaux and E. Rodriguez, "Le Van Quyen. M. Studying Single-Trials of Phase Synchronous Activity in the Brain," Int. J. Bifurc. Chaos **10**, 2429–2439 (2000).

58. A. Kraskov, *Synchronization and Interdependence Measures and Their Applications to the Electroencephalogram of Epilepsy Patients and Clustering of Data*, PhD Thesis (Research Centre Jlich, John von Neumann Inst. for Computing, 2004); http://www.fz-juelich.de/nic-series/volume24/nic-series-band24.pdf

59. C. Torrence and G. P. Compo, "A Practical Guide to Wavelet Analysis," Bull. Am. Meteorol. Soc. **79**, 61–78 (1998).

60. A. Ye. Hramov and A. A. Koronovskii, "An Approach to Chaotic Synchronization," Chaos **14**, 603–610 (2004).

61. L. Cimponeriu, M. Rosenblum, and A. Pikovsky, "Estimation of Delay in Coupling from Time Series," Phys. Rev. E. **70**, 046213 (2004).

62. C. W. J. Granger, "Investigating Causal Relations by Econometric Models and Cross-Spectral Methods," Econometrica **37**, 424–438 (1969).

63. K. J. Blinowska, R. Kus, and M. Kaminski, "Granger Causality and Information Flow in Multivariate Processes," Phys. Rev. E **70**, 050902 (2004).

64. W. Wang, B. T. Anderson, R. K. Kaufmann, and R. B. Myneni, "The Relation between the North Atlantic Oscillation and SSTs in the North Atlantic Basin," J. Clim. **17**, 4752 –4759 (2004).

65. B. M. Hallin and A. Saidi, "Testing Non-Correlation and Non-Causality between Multivariate ARMA Time Series," J. Time Series Analysis **26**, 83–105 (2005).

66. S. A. Aivazyan, *Statistical Study of Dependences* (Metallurgiya, Moscow, 1968) [in Russian].

67. G. Seber, *Linear Regression Analysis* (Wiley, New York, 1977; Mir, Moscow, 1974).

68. P. A. P. Moran, "Some Theorems on Time Series I," Biometrika **34**, 281–291 (1947).

69. A. S. Pikovsky, M. G. Rosenblum, and Yu. Kurhts, *Synchronization: Fundamental Nonlinear Phenomenon* (Tekhnosfera, Moscow, 2002) [in Russian].

70. URL: http://meto.gov.uk.

71. M. S. Bartlett, *Stochastic Processes* (Cambridge University Press, Cambridge, 1978).

72. I. I. Mokhov, "Climate Changes: Analyses of Global Cycles," Ann. Geophys. **12**, C334 (1993).

73. I. I. Mokhov, *Diagnosis of the Structure of the Climate System and Its Evolution in the Annual Cycle and Interannual Variability*, Doctoral Dissertation in Mathematical Physics (IFA RAN, Moscow, 1995).

Translated by N. Tret'yakova